

Thermal decomposition of a triangular-network sheet - A Molecular Dynamics simulation study

H. Popova¹, J. Paturej^{2,3}, A. Milchev^{1,2}, and T.A. Vilgis²

¹ *Institute for Physical Chemistry, Bulgarian Academy of Sciences, 1113 Sofia, Bulgaria*

² *Max Planck Institute for Polymer Research, 10 Ackermannweg, 55128 Mainz, Germany*

³ *Institute of Physics, University of Szczecin, Wielkopolska 15, 70451 Szczecin, Poland*

The thermal degradation of a graphene-like two-dimensional triangular membrane with bonds undergoing temperature-induced scission is studied by means of Molecular Dynamics simulation using Langevin thermostat. We demonstrate that the probability distribution of breaking bonds is highly peaked at the rim of the membrane sheet at lower temperature whereas at higher temperature bonds break at random anywhere in the hexagonal flake. The mean breakage time τ is found to decrease with the total number of network nodes N by a power law $\tau \propto N^{0.51}$ and reveals an Arrhenian dependence on temperature T . Scission times are themselves exponentially distributed. The fragmentation kinetics of the average number of clusters can be described by first-order chemical reactions between network nodes n_i of different coordination. The distribution of fragments sizes evolves with time elapsed from a δ -function through a bimodal one into a single-peaked again at late times. Our simulation results are complemented by a set of 1st-order kinetic differential equations for n_i which can be solved exactly and compared to data derived from the computer experiment, providing deeper insight into the thermolysis mechanism.

I. INTRODUCTION

Thermal degradation and stabilization of polymer systems has been a long-standing focus of research from both practical and fundamental viewpoints [1]. Plastic waste disposal has grown rapidly to ecological menace prompting researchers to investigate plastic recycling by degradation as an alternative [2]. On the other hand, degradation of polymers and other high molecular weight materials in different environments is usually a major limiting factor in their application. Thermal degradation (or, *thermolysis*) plays a decisive role in the design of flame-resistant polyethylene and other plastic materials [3]. Another interesting aspects for applications include reversible polymer networks [4, 5], and most notably, graphene, as a "material of the future" that shows unusual thermomechanical properties [6, 7]. Recently, with the rapidly growing perspective of exploiting bio-polymers as functional materials [8, 9] the stability of such materials has become an issue of primary concern [10, 11] as, e.g., that of double-stranded polymer decomposition [12].

Most theoretical investigations of polymer degradation have focused on determining the rate of change of average molecular weight [13–22]. The main assumptions of the theory are that each link in a long chain molecule has equal strength and equal accessibility, that they are broken at random, and that the probability of rupture is proportional to the number of links present. Therefore, all of the afore-mentioned studies investigate exclusively the way in which the distribution of bond rupture probability along the polymer backbone affects the fragmentation kinetics and the distribution of fragment sizes as time elapses. In a recent study [23], using Molecular Dynamics (MD) simulation with a Langevin thermostat, we observed a rather complex interplay between the polymer chain dynamics and the resulting bond rupture probability. A major role in this was attributed to the one-dimensional (1D) topological connectivity of the linear polymer.

To the best of our knowledge, however, we are not aware of any study so far of the thermal degradation kinetics in tethered (suspended) membranes (networks) with 2D topological connectivity. In the present work we extend our investigations to the case of (2D) polymer network sheets, embedded in 3D-space, and study as a generic example the thermal degradation of a suspended membrane with honeycomb orientation, similar to that of graphene.

The paper is organized as follows: after a brief introduction, we sketch our model in Sec. II where we introduce the basic quantities that are measured in the course of the simulation and explain the cluster-counting algorithm, developed for monitoring of the fragmentation process. A detailed description of the latter is given in the Appendix. In Sec. III we present our simulation results, that is, the distribution of bond scission rates over the membrane surface, the mean life time of a bond dependence on membrane size and temperature - cf. Sec. III A, the distribution of recombination events - Sec. III B, and the temporal evolution of the fragmentation process - Sec. III C. We also develop a theoretical scheme based on a set of 1st-order kinetic differential equations, describing the variation of the number of network nodes, connected by a particular number of bonds to neighboring nodes, as time elapses - Sec. IV. We demonstrate that the analytical solution of such system provides a faithful description of ... In Sec. V we conclude with a brief discussion of our main findings.

II. MODEL SYSTEM AND SIMULATION PROCEDURE

A. Model

We study a coarse-grained model of triangular membrane embedded in three-dimensional (3D) space. The membrane consists of N spherical particles (beads, monomers) of diameter σ connected in a honey-comb lattice structure whereby each monomer is bonded with three nearest-neighbors except of the monomers on the membrane edges which have only two bonds (see Fig. 1 [left panel]). The total number of monomers N in such a membrane is $N = 6L^2$ where by L we denote the number of monomers (or hexagonal cells) on the edge of the membrane (i.e., L characterizes the linear size of the membrane). There are altogether $N_{bonds} = (3N - 6L)/2$ bonds in the membrane. In our studies we consider *symmetric* hexagonal membranes (*flakes*) so as to minimize possible effects due to the asymmetric of edges or vortices at the membrane periphery.

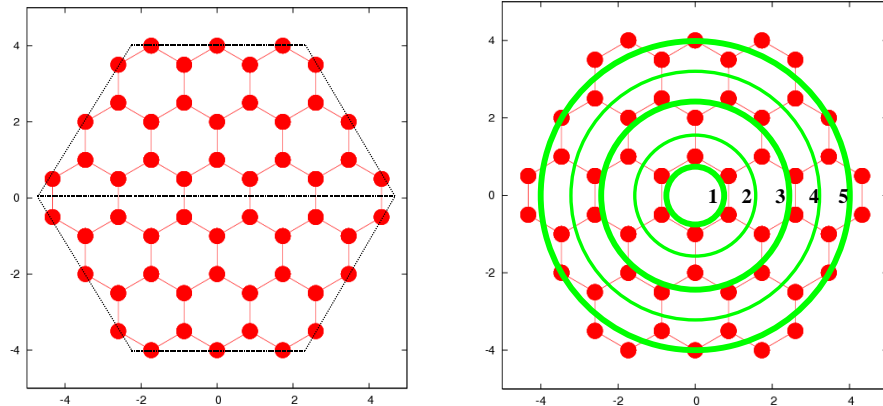


FIG. 1: [left panel] A model of a membrane with honey-comb structure that contains a total of $N = 54$ beads and has linear size $L = 3$ (L is the number of beads or hexagonal cells on the edge of the membrane). [right panel] An example of subdivision of beads and bonds, composing a membrane with $L = 3$, into subgroups (“circles”). The total number of circles C in the membrane of linear size L is $C = 2L - 1$.

We find it appropriate to divide the two-dimensional membrane network so that all the beads and bonds are distributed into different subgroups presented by concentric “circles” with consecutive numbers (see Fig. 1 [right panel]) proportional to the radial distance from the membrane center. To *odd* circle numbers thus belong beads and bonds that are nearly tangential to the circle. *Even* circles contain no beads and only radially oriented bonds (shown to cross the circle in Fig. 1). The total number of circles C in the membrane of linear size L is found to be $C = (2L - 1)$. We use this example of dividing the beads and the bonds composing membrane in order to represent our simulation results in appropriate way which relates them to their relative proximity to membrane’s periphery.

B. Potentials

The nearest-neighbors in the membrane are connected to each other by “breakable bonds” described by a Morse potential, where r is a distance between the monomers,

$$U_M(r) = \epsilon_M \{1 - \exp[-\alpha(r - r_{\min})]\}^2 \quad (1)$$

where $\alpha = 1$ is a constant that determines bond elasticity, $r_{\min} = 1$ is the equilibrium bond length. The dissociation energy of a given bond is $\epsilon_M = 1$, measured in units of $k_B T$, where k_B denotes the Boltzmann constant and T is the temperature. The minimum of this potential occurs at $r = r_{\min}$, $U_{\text{Morse}}(r_{\min}) = 0$. The maximal restoring force of the Morse potential, $f_{\max} = -dU_M/dr = \alpha\epsilon_M/2$, is reached at the inflection point, $r = r_{\min} + \alpha^{-1} \ln(2)$. This force f_{\max} determines the maximal tensile strength of the membrane. Since $U_M(0) \approx 2.95$, the Morse potential, Eq. (1), is only weakly repulsive and beads could partially penetrate one another at $r < r_{\min}$. Therefore, in order to allow properly for the excluded volume interactions between bonded monomers, we take the bond potential as a sum of $U_M(r)$ and the so called Weeks-Chandler-Anderson (WCA) potential, $U_{\text{WCA}}(r)$, (i.e., the shifted and truncated

repulsive branch of the Lennard-Jones potential),

$$U_{\text{WCA}}(r) = \begin{cases} 4\epsilon \left[\left(\frac{\sigma}{r}\right)^{12} - \left(\frac{\sigma}{r}\right)^6 \right] + \epsilon, & \text{for } r \leq 2^{1/6}\sigma \\ 0, & \text{for } r > 2^{1/6}\sigma \end{cases} \quad (2)$$

with parameter $\epsilon = 1$ and monomer diameter $\sigma = 2^{-1/6} \approx 0.89$ so that the minimum of the WCA potential coincides with the minimum of the Morse potential. Thus, the length scale is set by the parameter $r_{\text{min}} = 2^{1/6}\sigma = 1$. The nonbonded interactions between monomers are also taken into account by means of the WCA potential, Eq. (2). The nonbonded interactions in our model correspond to good solvent conditions whereas the bonded interactions make the bonds in our model breakable and they undergo scission at sufficiently high T .

C. MD algorithm

In our MD simulation we use a Langevin dynamics, which describes the Brownian motion of a set of interacting particles whereby the action of the solvent is split into slowly evolving viscous (frictional) force and a rapidly fluctuating stochastic (random) force. The Langevin equation of motion is the following:

$$m\dot{\vec{v}}_i(t) = \vec{F}_i(t) - m\gamma\vec{v}_i(t) + \vec{R}_i(t) \quad (3)$$

where m denotes the mass of the particles which is set to $m = 1$, \vec{v}_i is the velocity of particle i , $\vec{F}_i = (\vec{F}_M + \vec{F}_{\text{WCA}})_i$ is the conservative force which is a sum of all forces exerted on particle i by other particles in the system, γ is the friction coefficient and \vec{R}_i is the three dimensional vector of random force acting on particle i . The random force \vec{R}_i , which represents the incessant collision of the monomers with the solvent molecules, satisfies the fluctuation-dissipation theorem $\langle R_{i\alpha}(t)R_{j\beta}(t') \rangle = 2\gamma k_B T \delta_{ij} \delta_{\alpha\beta} \delta(t-t')$ where the symbol $\langle \dots \rangle$ denotes an equilibrium average and the greek-letter subscripts refer to the x , y or z components. The friction coefficient γ of the Langevin thermostat is set to $\gamma = 0.25$. The integration step is 0.002 time units (t.u.) and the time is measured in units of $r_{\text{min}} \sqrt{m/\epsilon_M}$. We emphasize at this point that in our coarse-grained modeling no explicit solvent particles are included. In this work the velocity-Verlet algorithm is used to integrate the equations of motion.

Our MD simulations are carried out in the following order. First, we prepare an equilibrated membrane conformation, starting with a fully flat configuration, Fig. 1, where each bead in the network is separated by a distance $r_{\text{min}} = 1$ equal to the equilibrium separation of the bond potential ($U_M + U_{\text{WCA}}$) [see Eq. (1) and (2)]. Then we start the simulation with this prepared conformation and let the membrane equilibrate in the heat bath at a temperature low enough that the membrane stays intact, Fig. 2, (this equilibration is done in order to prepare different starting conformations for each simulation). Once the equilibration is finished, the temperature is raised to the working one and we let the membrane equilibrate at this temperature for a while (roughly, ~ 20 t.u.). Then the time is set to zero

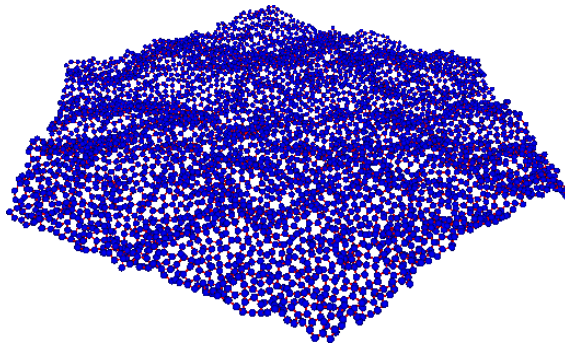


FIG. 2: A snapshot of a typical conformation of an intact membrane with $L = 30$ containing 5400 monomers after equilibration. Typical ripples are seen to cross the surface.

and we continue the simulation of this well-equilibrated membrane conformation to examine the thermal scission of the bonds. We measure the elapsed time τ until the first bond rupture occurs and repeat the above procedure for a large number of events ($10^3 \div 10^4$) so as to sample the stochastic nature of rupture and to determine the mean $\langle \tau \rangle$ which we refer to as the mean first breakage time (MFBT). In the course of simulation we also calculate properties

such as the probability distribution of breaking bonds regarding their position in the membrane (a rupture probability histogram), the probability distribution of the first breakage time $W(\tau)$ (a life time probability distribution), the strain (extension) of the bonds with respect to the consecutive circle number in the membrane, as well as other quantities of interest.

Since in the problem of thermal degradation there is no external force acting on the membrane edges, a well-defined activation barrier for a bond scission is actually missing, in contrast to the case of applied tensile force. Therefore, a definition of an unambiguous criterion for bond breakage is not self-evident. Moreover, depending on the degree of stretching, bonds may break and then recombine again. Therefore, in our numeric experiments we use a sufficiently large value for critical extension of the bonds, $r_h = 5r_{\min}$, which is defined as a threshold to a broken state of the bond. This convention is based on our checks that the probability for recombination (self-healing) of bonds, stretched beyond r_h , is sufficiently small, $< 10^{-5}$.

Also we examine the course of the degradation kinetics: at periodic intervals we analyze the size distribution of fragments (clusters) of the initial membrane and establish the time-dependent probability distribution function of fragment sizes, $P(n, t)$, as time elapses after the onset of the thermal degradation process. This also yields the time evolution of the mean fragment size, $N(t) = \int_0^\infty n(t)P(n, t)dt$. We perform the statistical averaging of fragment sizes by developing an appropriate for the system fast cluster counting algorithm which is given in the Appendix A.

D. Cluster Counting Algorithm

The Molecular Dynamics calculations were carried out using a cluster counting algorithm based on an *ad hoc* implementation of the Hoshen-Kopelman program [26] which in the present realization is written in C.

The introduction of the Hoshen-Kopelman algorithm [26] in 1976 was an important breakthrough in the analysis of cluster size statistics in percolation theory. The majority of the Hoshen-Kopelman algorithm adaptations and implementations, however, were designed for lattice environments (discrete systems). Only a few studies discussed the Hoshen-Kopelman algorithm implementation in non-lattice environments (continuous systems). In such systems, the positions of the sites are arbitrary, and not restricted to the discrete points of a regular lattice.

In the paper of Al-Futaisi and Patzek [27] in 2003, the Hoshen-Kopelman algorithm for cluster labeling has been extended to non-lattice environments where network elements (sites or bonds) are placed at random points in space. This extension of the Hoshen-Kopelman algorithm is not restricted to a non-lattice environment, and can be applied to lattices in two, three or higher dimensions. It can also be applied to networks consisting of sites (nodes), bonds, or both, and each site can have a different number of connecting bonds. So, clusters of sites, bonds, or sites-and-bonds in such a complex arbitrary network can be labeled with this implementation of the Hoshen-Kopelman algorithm. Following Al-Futaisi and Patzek [27], we developed our simplified version of this algorithm which concerns only clusters of nodes in a network with hexagonal (honey-comb) structure (which is our model shown in Fig. 2).

III. MD-RESULTS

A. Mean life time τ

In Fig. 3a we show the distribution of bond scission rate among all bonds of the honeycomb membrane for flakes of several sizes $L = 10, 15, 20$. Somewhat surprisingly, one finds the the overwhelming fraction of bond breaking occurs at the outer-most rim of the membrane where monomers are bound by only two bonds to the rest of the sheet. The difference in the relative stability of the bonds becomes clearly evident in Fig. 3b where the the frequency of periphery bonds appears nearly two orders of magnitude larger when compared bonds in the 'bulk' of the membrane where each monomer (node) is connected by three bonds to its neighbors. One may therefore conclude that a moderate increase in the coordination number of the nodes (by only 33%) leads to a major stabilization of the supporting bonds and much stronger resistance to fracture.

The variation of the mean life time τ of a bond with membrane size N during thermolysis is displayed in Fig. 4a. Evidently, one observes for τ , which can be considered also as a mean First Breakage Time (MFBT), a well pronounced power law behavior, $\tau \propto N^{-\beta}$ with an exponent $\beta \approx 0.51 \pm 0.03$. This value of β might appear somewhat surprisingly to deviate from the expected exponent of unity, given that in the absence of external force all bonds are supposed to break completely at random so that the total probability for a bond scission (i.e., the chance that *any* bond might break within a time interval) is additive and should be, therefore, proportional to the total number of available bonds, $N_{bonds} = (3N - 6L)/2$. As suggested by Fig. 3, however, predominantly only periphery bonds are found to undergo scission during thermal degradation. The number of periphery bonds goes roughly as $\propto \sqrt{N}$ which agrees well with the observed value $\beta \approx 0.51$ and provides a plausible interpretation of the simulation result, Fig. 4a. From

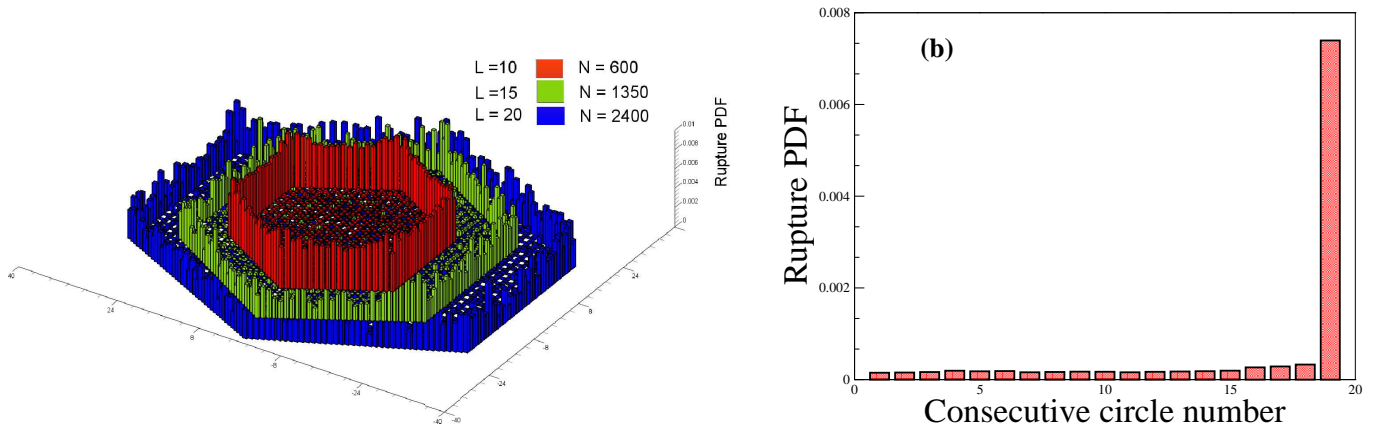


FIG. 3: (a) Rupture probability histograms for thermally induced scission events in flexible honeycomb membrane of different linear size L as shown in the legend. Parameters of the heat bath are $T = 0.1$ and $\gamma = 0.25$. (b) Probability distribution of breakage events as a function of consecutive circle number for a membrane with $N = 600$, $L = 10$.

the inset in Fig. 4a one may verify that the bond scission displays an Arrhenian dependence on inverse temperature, $\tau \propto \exp(\Delta E_b/k_B T)$, with a slope $\Delta E_b/k_B T \approx 1$ which is an activation energy barrier ΔE_b of the order of the potential well depth of the Morse interaction, Eq. (1) where $\epsilon_M = 1.0$.

The probability distribution function (PDF) of MFBT $W(t)$, i.e., the PDF of the time interval before the first breakage event in the membrane takes place, is shown in Fig. 4b for $T = 0.1$. Evidently, one has $W(t) \propto \exp(-t/\tau)$ with a sharp maximum close to $t \approx 0$. At even lower temperature one might expect this maximum to become more pronounced, suggesting thus a Poisson distribution for the $W(t)$. As far as τ tends to grow exponentially fast with

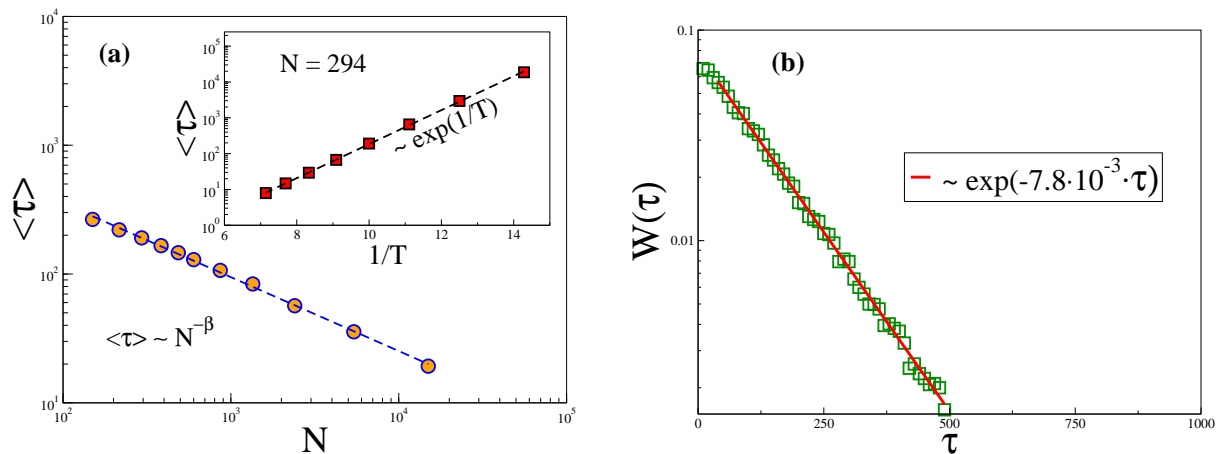


FIG. 4: (a) Mean first breakage time $\langle \tau \rangle$ vs. number of beads N in the membrane. Dashed line represents a fit by power law with an exponent $\beta = 0.51$. The inset shows the variation of $\langle \tau \rangle$ with inverse temperature $1/T$ for a membrane with $N = 294$ particles. The fitting line yields an Arrhenian relationship, $\langle \tau \rangle \propto \exp(\Delta E_b/k_B T)$ with activation energy barrier $\Delta E_b \approx 0.95$. (b) Lifetime probability distributions $W(t)$ for thermally induced breakage of a membrane with $N = 600$ particles at $T = 0.1$. Symbols denote result of the simulation and full line stands for a fitting function $W(t) \propto \exp(-t/\tau)$.

decreasing T - see inset in Fig. 4a, collecting statistics in this temperature range becomes difficult.

B. Bond recombination

It has been mentioned in Section II that in the absence of external force acting on the membrane the criterion for a bond to be considered broken is not unambiguous. Adopting a rather large critical bond extension of $r_h = 5r_{min}$

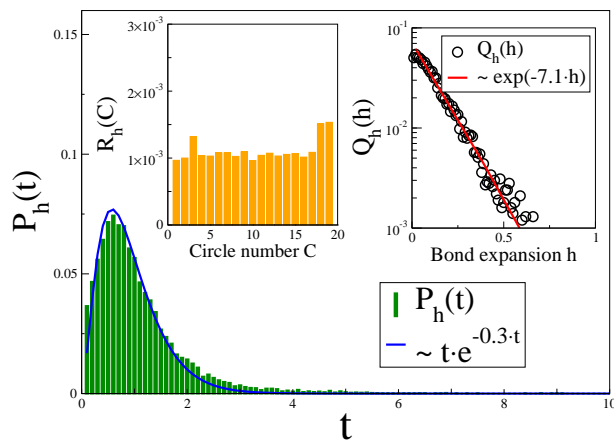


FIG. 5: Probability distribution $P_h(t)$ of times (impulses), and $Q_h(h)$ of maximal bond lengths h (circles, right panel of inset) before a recombination event in a membrane with $N = 600$, $T = 0.1$, $\gamma = 0.25$ takes places. The recombination times probability distribution $P_h(t)$ is fitted by Poisson distribution (blue line). The probability for a bond stretching a distance h is described by $Q_h(h)$ indicating an exponential decay - red line. The left inset shows healing probability R_h vs. consecutive *circle* number, demonstrating which part of the membrane undergoes healing most frequently.

almost rules out the probability of subsequent recombination of such bonds, as indicated by $Q_h(h) \propto \exp(-7.1h)$ in Fig. 5 (right inset). We find that less than 2% of the overstretched bonds reach $\approx 0.14r_{min}$ before recombination. The PDF $P(t)$ of times elapsed before self-healing is also shown in Fig. 5 where appears as a Poisson distribution, $P(t) \approx t \exp(-0.3t)$. Not surprisingly, most of the broken bond that recombine occur in the periphery of the membrane - left inset in Fig. 5.

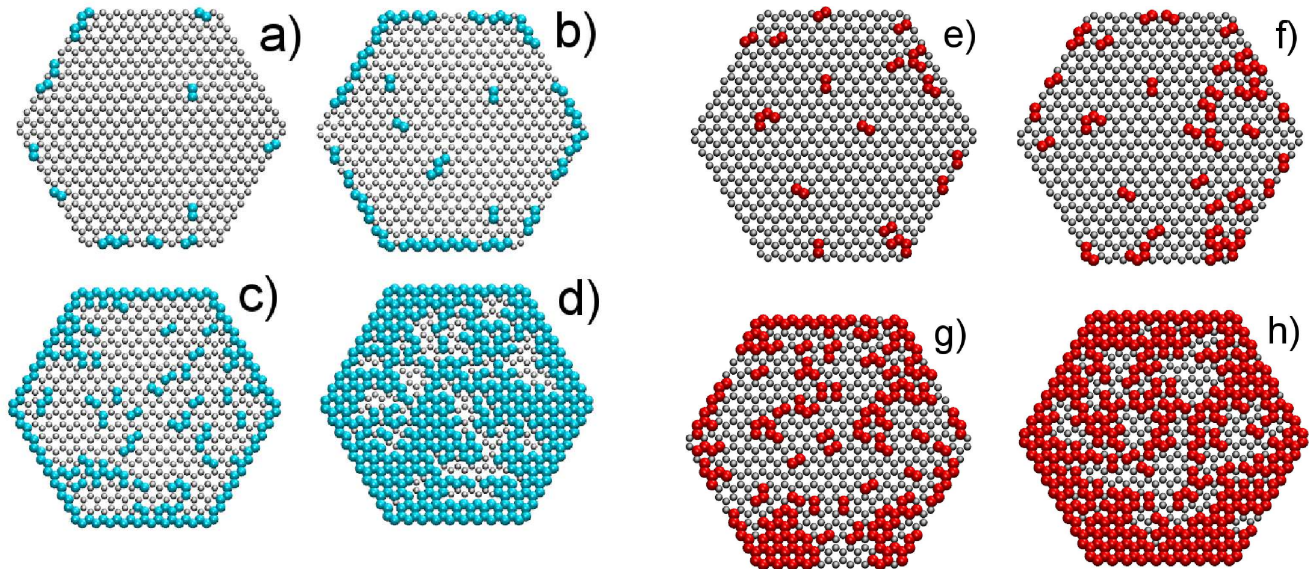


FIG. 6: Thermal breakage of bonds in a membrane made of $N = 600$ particles at different time moments: a) $t = 10^2$, b) $7 \cdot 10^2$, c) $5 \cdot 10^4$, d) $3 \cdot 10^5$ and e) 50, f) 100, g) 250, h) 500. Broken bonds are marked by blue ($T = 0.1$) or red ($T = 0.15$) color, depending on the temperature of a heat bath, while gray color corresponds to intact bonds.

In Fig. 6 we show the distribution of broken bonds at different times after the onset of thermal degradation. Two different temperatures, $T = 0.10$ and $T = 0.15$ are studied. One can readily verify from Fig. 6a-d that at $T = 0.10$ the degradation process starts from the rim of the triangular network sheet and then proceeds inwards, as noted earlier by Meakin[25]. In contrast, at 50% higher temperature, i.e., at $T = 0.15$, bonds break indiscriminately anywhere in the

network sheet - cf. Fig. 6b, f and Fig. 6c, g. Such difference in the bond scission mechanism at different temperatures has been observed [25] too. It appears that at low T only the membrane periphery undergoes local oscillations that lead to bond scission while in the inner part of the sheet the monomers mutually block each other and the bonds remain largely intact. A 'hot' membrane undergoes much stronger agitation as a whole and as a result bonds break all over the network sheet. Indeed, at lower T when the thermal agitation of the membrane is weaker, one may correlate the probability of bond scission with the average strain in the bonds - Fig. 7. Evidently, the average squared bond

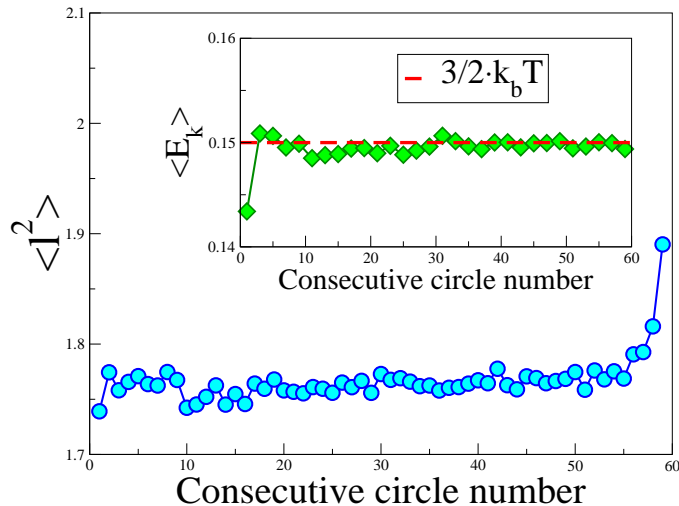


FIG. 7: Variation of mean squared bond length $\langle l^2 \rangle$ vs. distance from membrane center (consecutive circle number) for thermolysis of membrane composed of $N = 5400$ beads. The inset displays mean kinetic energy $\langle E_k \rangle$ (per monomer) as a function of circle number. Red dashed line represents the level of energy which corresponds to equipartition theorem. Parameters of thermostat are $T = 0.1$ and $\gamma = 0.25$.

length $\langle l^2 \rangle$ increases steadily and becomes nearly 8% larger for the bonds sitting on the last ring of the membrane whereas no difference in the mean kinetic energy between peripheral and bulk nodes is detected - Fig. 7. Note, that the kinetic energy (that is, the temperature T) is thereby uniformly distributed along the sheet - see inset in Fig. 7.

C. Temporal evolution of the fragmentation process

After the onset of the thermal decomposition process the membrane flake disintegrates into smaller clusters (fragments) of size n whose mean size (or, molecular weight) $N(t)$ decreases steadily with time. $N(t)$ is easily accessible experimentally, therefore we give in Fig. 8a the course of its temporal evolution, observed in our computer experiment. Using an *ad hoc* cluster counting program in the course of the MD-simulation, we sample the probability distribution of fragment sizes, $P(n, t)$, so that the first moment $N(t) = \int n(t)P(n, t)dt$ gives the cluster mean size $N(t)$. Thus, for a given time moment t we average data over more than 10^3 independent runs, each starting from a different initial conformation of the honeycomb membrane. In Fig. 8b we show the time variation of the ensuing PDF $P(n, t)$ whereby the system is seen to start with a single sharp peak at $t = 0$ when the membrane is still intact. As time goes by $P(n, t)$ becomes bimodal, the maximum of the distribution is seen to shift to smaller values of cluster size whereas an accumulation of fragments of size 1 or 2 is observed to a second peak at $n \approx 1$. Eventually, as $t \rightarrow \infty$, the PDF $P(n, t)$ settles to a shape with a single sharp peak at $n \approx 1$ (not shown here).

One can readily see from Fig. 8a that the quantity $1 - N^{-1}(t)$ does not immediately follow a straight line of decay when plotted in semi-logarithmic coordinates, rather, such a decay is observed after an initial period of slower decline. This effect is due to averaging over many realizations of the fragmentation process. In each run the degradation of bonds starts earlier or later at a particular time τ (the First Passage Time) that is distributed according to $W(\tau)$ - cf. Fig. 4b. As a result a clear cut exponential course of $1 - N^{-1}(t)$ is only observed in the late stages of fragmentation. Such behavior is found independently of the membrane size - Fig. 8a.

In addition, one could expect that the fragmentation process is not governed by a single rate constant in a presumably 1^{st} -order chemical reaction even though the bonds that undergo rupture are chemically identical. Therefore, from the temporal mean cluster size behavior, presented in Fig. 8a, one may conclude that even in the case of a homogeneous membrane the thermal degradation process is more adequately described by several reaction constants which govern

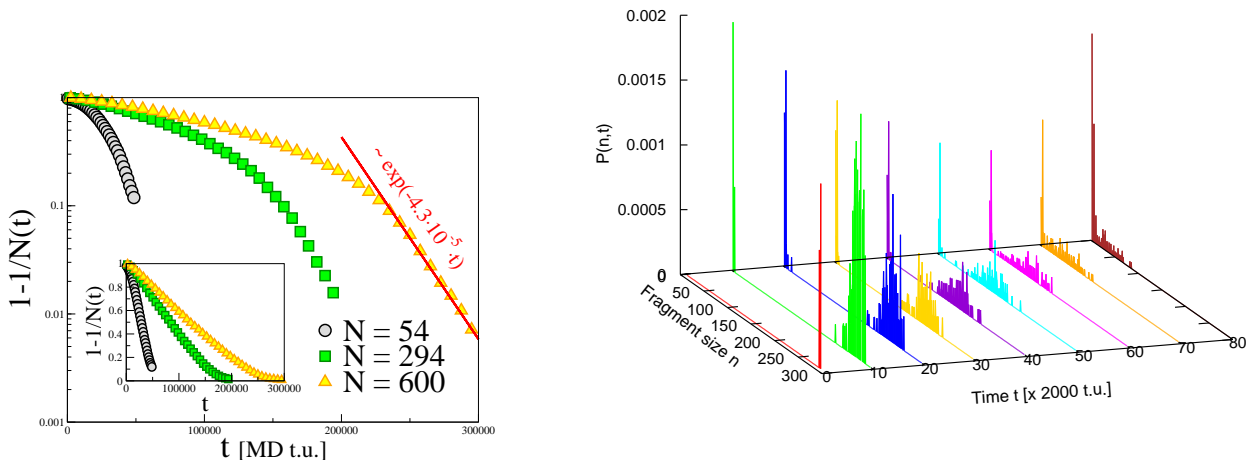


FIG. 8: (a) Semi-log plot of time variation of mean fragment size $N(t)$ for membranes made of different size as indicated. Symbols represent simulation results whereas a red line stands for the fitting function $1 - 1/N(t) \propto \exp(-kt)$. The kinetic constant $k = 4.3 \cdot 10^{-5} \text{ s}^{-1}$. In the inset the same is shown in normal coordinates. (b) Probability distribution of fragment sizes $P(n, t)$ at different times t (in MD time units) after beginning of the thermal degradation process for a membrane with $N = 294$. Parameters of a heat bath are $T = 0.12$ and $\gamma = 0.25$.

the dissociation of different groups of bonds. In the next section we suggest a simple model of reaction kinetics which takes into account this conjecture.

IV. REACTION KINETICS

One may try to reproduce the bond scission kinetics during in the course of thermal fragmentation as a set of several 1^{st} -order chemical reactions. The nodes of the membrane can be subdivided into several groups, depending on the number of intact bonds that connect them to neighboring nodes. In the case of a honeycomb membrane one may distinguish four such groups, and denote the instantaneous number of such nodes (monomers) by n_0 , n_1 , n_2 and n_3 whenever 0, 1, 2, or 3 intact bonds exist around such a node. If self-recombination of bonds is ignored, which is reasonable, according to Fig. 5, one can write down a strongly simplified set of 1^{st} -order kinetic differential equations (DE) that describes the evolution of $n_0(t)$, $n_1(t)$, $n_2(t)$ and $n_3(t)$ with time:

$$\begin{aligned} \dot{n}_1(t) &= -k_1 n_1(t) + k_2 n_2(t) \\ \dot{n}_2(t) &= -k_2 n_2(t) + k_3 n_3(t) \\ \dot{n}_3(t) &= -k_3 n_3(t) \end{aligned} \quad (4)$$

Thus, for example, the number of double-bonded nodes decreases as one of the two bonds breaks, however, if a bond breaks around a node with triple coordination this would increase the population of double-bonded nodes too. Note, that the total number of nodes of all kinds remains thereby conserved,

$$n_0(t) + n_1(t) + n_2(t) + n_3(t) = N = 6L^2. \quad (5)$$

If the degradation process starts with an intact membrane conformation at $t = 0$ (no broken bonds exist), one can fix the initial conditions as $n_0(0) = 0$, $n_1(0) = 0$, $n_2(0) = 6L$ and $n_3(0) = N - n_2(0) = 6L(L - 1)$. Thus, initially one has only $n_2(0) = 6L$ double-bonded nodes at the membrane periphery along with $n_3(0) = 6L(L - 1)$ triple-bonded nodes in the bulk of the flake. Then, as the decomposition process develops, nodes from a given class $r = 1, 2, 3$ will transform into a lower class $r = 0, 1, 2$ ones (we neglect hereby the simultaneous scission of more than one bond of a node as highly improbable event). Eventually, at $t \rightarrow \infty$ the fragmentation process ends and one expects $n_1(\infty) = n_2(\infty) = n_3(\infty) = 0$ and $n_0(\infty) = N$.

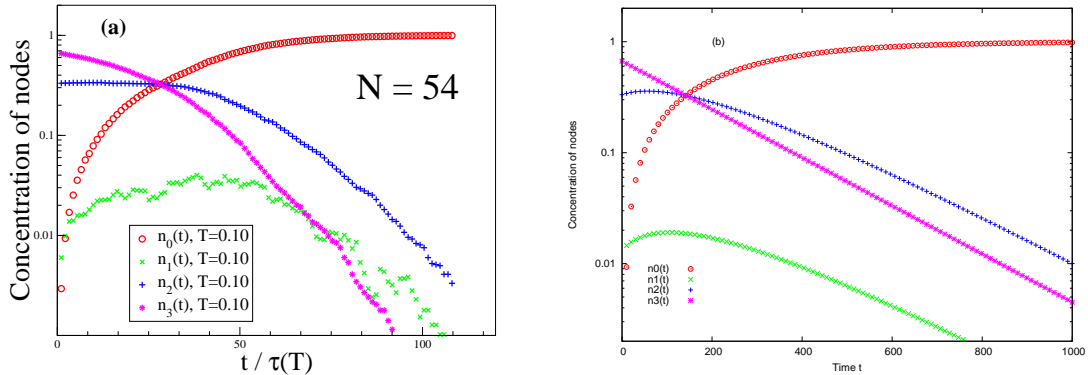


FIG. 9: (a) Variation of the number of nodes $n_m(t)$ with $m = 0 \div 3$ intact bonds with elapsed dimensionless time $t/\tau(T)$ for a membrane with $N = 54$ and two different temperatures $T = 0.10$ (lines) and $T = 0.15$ (symbols). Here $\tau(T)$ denotes the characteristic time of degradation at the respective temperature T . The $n_1(t)$ (monomers bound by a single bond) are shown by shaded area. (b) The same as in (a) for the same membrane size $N = 54$ according to the analytic result Eqs. (6). The values of the kinetics rate constants are $k_1 = 20.0$, $k_2 = 0.007$, $k_3 = 0.005$.

One may solve analytically the system of 1st-order DE (4) to a set of functions $n_i(t)$ with $0 \leq i \leq 3$:

$$\begin{aligned}
 n_0(t) &= 6L^2 - n_1(t) - n_2(t) - n_3(t) \\
 n_1(t) &= \frac{6L}{(k_1 - k_2)(k_1 - k_3)(k_2 - k_3)} \left[k_1(k_2 - k_3)(e^{-k_3t} - e^{-k_1t}) + k_2k_3(e^{-k_3t} - e^{-k_2t}) \right. \\
 &\quad \left. + k_1k_3L(e^{-k_3t} - e^{-k_2t}) - k_2k_3L(e^{-k_3t} - e^{-k_1t}) + k_3^2L(e^{-k_2t} - e^{-k_1t}) \right] \\
 n_2(t) &= 6L \frac{(k_2e^{-k_2t} - k_3e^{-k_3t} - k_3Le^{-k_2t} + k_3Le^{-k_3t})}{k_2 - k_3} \\
 n_3(t) &= 6L(L - 1)e^{-k_3t}
 \end{aligned} \tag{6}$$

where the rate constants k_1 , k_2 and k_3 are still to be determined, for example, by comparison with simulation data. As one may readily verify from Fig. 3, our simulation data suggest that a bond to a triple-bonded node at $T = 0.12$ is much more stable (by about two orders of magnitude) than a bond at the flake periphery where each node is connected by only two bonds to the network. Thus the system of Eqs. (6) can be tested for a set of reaction constants $k_1 \gg k_2 > k_3$ directly by means of our Molecular Dynamics computer experiment.

Indeed, one finds by comparing the simulation result, Fig. 9a for a membrane of size $N = 54$ at $T = 0.10$, and the analytical solution, Eqs. (6), Fig. 9b, that the observed kinetics agree qualitatively, provided one allows for the absence of fluctuation in Eqs. (4) (i.e., for the disarray and averaging of the First Passage Times τ in the simulation data). We should like to point out here that the values of the rate constants k_1 , k_2 , k_3 are *not* best fit values but rather the first physically reasonable numbers that produce a picture resembling Fig. 9a.

One may conclude therefore that the simplified set of 1st-order DE (4) captures qualitatively the main features of the fragmentation kinetics and the principal mechanism at work is a combination of few 1st-order chemical reactions of bond scission. Nonetheless, it is conceivable to expect that for a full quantitative description of the thermal degradation process the set of kinetic equations, Eqs. (4), should be extended by few additional reactions: $n_1(t) \rightarrow n_2(t)$, $n_2(t) \rightarrow n_3(t)$ that may in principle also take place (with respective rate constants). One can then still derive an analytical solution of the extended set of DE that describes the full kinetics of fragmentation and try to fit the ensuing rate constants to the simulation data. In view of the growing number of fit parameters, however, a detailed analysis of such system is beyond the scope of the present work and should be left for future work.

V. SUMMARY

In the present investigation we use Langevin Molecular Dynamics simulation and also solve a simplified set of 1st-order kinetic DE so as to model the process of thermal destruction of a polymerized membrane sheet with honeycomb structure. Our findings regarding the most salient features of thermolysis in a breakable elastic network sheet subject to sufficiently high temperature can be summarized as follows:

- The probability of bond scission is highest at the periphery of the membrane sheet where nodes are connected by two bonds only. At higher temperature, however, the whole sheet undergoes fragmentation whereby also bonds in the bulk rupture.
- The mean first breakage time τ until a bond undergoes scission event declines with the number of nodes N (membrane size) by a power law as $\tau \propto N^{-0.51}$ and the times of bond scission are exponentially distributed, $W(t) \propto \exp(-t/\langle\tau\rangle)$.
- Bond recombination (self-healing) occurs seldom during thermal degradation, and the measured recombination times follow Poisson distribution whereas extra-stretching of bonds (beyond the point of maximal tensile strength) before a recombination takes place is exponentially probable.
- the fragmentation kinetics is determined by 1st-order reactions between network nodes with different number of intact bonds and follows simple exponential decay at late times.
- A set of 1st-order kinetic differential equations, describing the process of fragmentation, can be established and solved analytically. One finds results in qualitative agreement with those from computer experiment providing thereby a deeper insight into the mechanism of thermal degradation of two-dimensional triangular networks.

In view of the presented results, it should be clear that more work is needed until a full understanding of the process of thermal degradation in polymerized 2d-membranes is reached.

VI. ACKNOWLEDGMENTS

A. M. gratefully acknowledges support by the Max-Planck-Institute for Polymer Research during the time of this investigation. This study has been supported by the Deutsche Forschungsgemeinschaft (DFG), Grant Nos. SFB625/B4 and FOR597.

-
- [1] N. S. Allen and M. Edge, *Fundamentals of Polymer Degradation and Stabilization*, Elsevier Applied Science, New York, 1966.
- [2] G. Madras, J. M. Smith, and B. J. McCoy, *Ind. Eng. Chem. Res.*, (1996) **35**, 1795.
- [3] M. R. Nyden, G. P. Forney, and G. E. Brown, *Macromolecules*, (1992) **25**, 1658.
- [4] R. P. Sijbesma, F. H. Beijer, L. Brunsveld, B. J. B. Folmer, J. H. K. K. Hirschberg, R. F. Lange, J. K. L. Lowe, and E. W. Meijer, *Science*, (1997) **278**, 1601.
- [5] R. P. Sijbesma and E. W. Meijer, *Chem. Commun.*, (2003) **1**, 5.
- [6] M. Neek-Amal and F. M. Peeters, *Phys. Rev. B* (2010) **81**, 235437; *Phys. Rev. B* (2010) **82**, 085432; *Appl. Phys. Lett.* (2010) **97**, 153118.
- [7] H. Zhao, K. Min and N. R. Aluru, *Nano Letters* (2009) **9** (8) 3012; H. Zhao and N. R. Aluru, *Jour. Appl. Phys.* (2010) **108**, 064321; K. Min and N. R. Aluru, *Appl. Phys. Lett.* (2011) **98**, 013113.
- [8] M. Sarikaya, C. Tamerler, A. K. Jen, K. Schulten, and F. Banyex, *Nature Mater.* (2003) **2**, 577.
- [9] T. H. Han, J. Kim, J. S. Park, C. B. Park, H. Ihee, and S. O. Kim, *Adv. Mater.* (2007) **19**, 3924.
- [10] T. Lindahl, *Nature* (London), (1993) **362**, 709.
- [11] R. P. Sinha and D.-P. Hader, *Photochem. Photobiol. Sci.* (2002) **1**, 225.
- [12] W. V. Metanomski, R. E. Bareiss, J. Kahovec, K. L. Loening, L. Shi and V. P. Shibaev, *Pure Appl. Chem.* (1993) **65**, 1561.
- [13] H. H. G. Jellinek, *Trans. Faraday Soc.* (1944) **1944**, 266.
- [14] M. Ballauff and B. A. Wolf, *Macromolecules*, (1981) **14**, 654.
- [15] R. M. Ziff and E. D. McGrady, *Macromolecules* (1986) **19**, 2513; E. D. McGrady and R. M. Ziff, *Phys. Rev. Lett.* (1987) **58**, 892.
- [16] Z. Cheng and S. Redner, *Phys. Rev. Lett.* (1988) **60**, 2450.
- [17] E. Blaisten-Barojas and M. R. Nyden, *Chem. Phys. Lett.* (1990) **171**, 499; M. R. Nyden and D. W. Noid, *J. Phys. Chem.* (1991) **95**, 94.
- [18] T. P. Doerr and P. L. Taylor, *J. Chem. Phys.* (1994) **101**, 10107.
- [19] M. Wang, J. M. Smith, and B. J. McCoy, *AIChE Journal*, (1995) **41**, 1521.
- [20] B. C. Hathorn, B. G. Sumpter, and D. W. Noid, *Macromol. Theory Simul.* (2001) **10**, 587.
- [21] P. Doruker, Y. Wang, and W. L. Mattice, *Comp. Theor. Polym. Sci.* (2001) **11**, 155.
- [22] M. B. Flegg, P. K. Pollett and D. K. Gramotnev, *Phys. Rev. E*, (2008) **77**, 021105; *Phys. Rev. E* (2008) **78**, 031117.
- [23] J. Paturej, A. Milchev, V. G. Rostiashvili, and T. A. Vilgis, *J. Chem. Phys.* (2011) **134**, 224901; *EPL* (2011) **94** 48003.
- [24] C. L. Dias, J. Kröger, D. Vernon, and M. Grant, *Phys. Rev. E* (2009) **80**, 066109.

- [25] Meakin, P. and Z. Xu, "Dissipative particle dynamics and other particle methods for multiphase fluid flow in fractured and porous media," *Progress in Computational Fluid Dynamics* (2009) **9** (6/7): 399, doi:10.1504/PCFD.2009.027371.
- [26] J. Hoshen, R. Kopelman, (1976) *Phys. Rev. B* **14** 3438.
- [27] Ahmed Al-Futaisi, Tadeusz W. Patzek, *Physica A* (2003) **321** 665.

APPENDIX: A *C*-function for cluster counting

Here, we provide the complete version of the function "CLUSTER_COUNT()" written in the *C* programming language that performs our simplified implementation of the extended Hoshen-Kopelman algorithm and calculates cluster statistics in lattice and non-lattice environments. This our implementation works for network with a hexagonal (honey-comb) structure (as shown in Fig. 1) where each node can have maximum three connecting bonds with the nearest-neighboring nodes. But this our function "CLUSTER_COUNT()" can be easily changed to be applied for network with arbitrary connectivity between the nodes (triangular, square, and so on structure).

In our implementation of the Hoshen-Kopelman algorithm we assume that all nodes and all links in the network are occupied, but some links can be broken when we study thermal degradation process of the network. The network information is stored in two arrays. The first one is related to the connectivity of the nodes and the second to the state of links (intact or broken link). The connectivity of the nodes in the network is described through the Bond_Neighbor array. In this array, we define the neighboring nodes that are directly connected to each node. The size of this array is the total number N of nodes in the network by the maximum connectivity or the coordination number (which is 3 in a honey-comb network). Therefore for the nodes that have coordination number less than the maximum we define their appropriate neighboring nodes and assign minus one (-1) to the remaining array elements (such are the periphery nodes on the edges of our hexagonal network which have only 2 connections with neighboring nodes). The array bond_rupture describes the state of each bond. If the bond is intact, we assign zero, otherwise when the bond is broken, we assign one. With these data structures in hand, we are ready to describe our implementation of the Hoshen-Kopelman algorithm. We follow the description of the algorithm given by Al-Futaisi and Patzek [2], and our implementation is described in six steps. In Step 1, read the network data structures - the input (global) arrays Bond_Neighbor and bond_rupture. In Steps 2 and 3, initialize the output variables - arrays NodeL and NodeLP. Then traverse the network in Step 4, and at each node, i , elements in NodeL and NodeLP are changed according to the following conditions: (4.1) if the node does not have any links together with its adjacent (neighboring) nodes, then start a new cluster (and record this new cluster in NodeL and NodeLP); (4.2) if the node has at least one link, then we define two possibilities: (i) If none of the neighboring nodes is labeled, then start a new cluster (and update NodeL and NodeLP, accordingly); (ii) If there exists a labeled neighbor and its link also exists, then set NodeL of the node and NodeLP of the neighboring nodes equal to the minimum of NodeLP[NodeL[j]] of the neighboring nodes j . After the scan in Step 4 is completed, in Step 5 operate only on the array NodeLP, and renumber labels in NodeLP to be sequential. In Step 6, apply the corrected labels in NodeLP to the array NodeL. Just as for the classic Hoshen-Kopelman algorithm on lattices, the extended algorithm on continuum systems is completed in a single pass through the nodes of the network and cluster relabeling operates on a vector whose size is much smaller than the size of the network.

```
void CLUSTER_COUNT(long N)
{
    /*=====
    COUNT CLUSTERS IN A NETWORK CONFIGURATION (a honey-comb structure): Extension
    of Hoshen-Kopelman's' cluster labeling algorithm to non-lattice environment
    =====*/

    /* Local variables */
    long i, nn1, nn2, nn3, link1, link2, link3, L_nn1, L_nn2, L_nn3;
    long cluster_counter, cn, i_cn, NodeLPmin;
    long NumberOfClusters, max_cluster_number, cluster_number, num_mono;
    long Num_cl[4];

    /* Input arguments: -----
    N          - Number of nodes (monomers) in the network
    Bond_Neighbour[][] - Neighboring nodes connected to each node
    bond_rupture[i][j] - State of the bond (0-intact/1-broken) between
    monomers i and j
```

Output arguments:

NumberOfClusters - Number of occupied clusters
 NodeL[] - Array to store cluster labels of nodes
 NodeLP[] - Array that holds information about the cluster labels

```

=====*/
// STEP 1: READ THE DATA AND INITIALIZE THE OUTPUT
  NumberOfClusters = 0;

// STEP 2: INITIALIZE THE HOSHEN-KOPELMAN ALGORITHM VARIABLES - array NodeL
  for (i = 0; i < N; i++) NodeL[i] = 0;

// STEP 3: CREATE EMPTY ARRAY NodeLP AND START CLUSTER COUNTER
  for (i = 0; i <= N; i++) NodeLP[i]=0;
  cluster_counter=0; // Cluster counter

// STEP 4: SCAN THE NETWORK NODES
  // i - the number of the current monomer
  // nn1, nn2, nn3 - the numbers of the bonded neighbors of the current
  monomer

  for (i = 0; i < N; i++) { //loop over all monomers
    //take the bonded neighbors of each monomer
    nn1 = Bond_Neighbour[i][0]; //take the number of the 1st-bonded neighbor
    of i-th monomer
    nn2 = Bond_Neighbour[i][1]; //take the number of the 2nd-bonded neighbor
    of i-th monomer
    nn3 = Bond_Neighbour[i][2]; //take the number of the 3th-bonded neighbor
    of i-th monomer

    //chek for bond ruptures of i-monomer: link=1 - broken bond (bond
    rupture); link=0 - intact (unbroken) bond;
    link1 = bond_rupture[i][nn1];
    link2 = bond_rupture[i][nn2];
    if (nn3 != -1) { //(nn3=-1) when the periphery monomer has only 2 bonded
    neighbors (instead of 3)
      link3 = bond_rupture[i][nn3];
    }
    else link3 = 1;

    // If this node is type (4.1) - all its links are broken!
    if (link1==1 && link2==1 && link3==1)
    {
      cluster_counter +=1; // Start a new cluster
      NodeL[i]=cluster_counter;
      NodeLP[cluster_counter]=cluster_counter;
    } // end if (end case 4.1)

    // This node is of type (4.2) - it has at least one intact link!
    else
    {
      L_nn1 = NodeL[nn1];
      L_nn2 = NodeL[nn2];
      if(nn3 != -1) L_nn3 = NodeL[nn3]; else L_nn3 = 0;

      // Case 4.2 (i): No neighbour is already labeled
      if (L_nn1==0 && L_nn2==0 && L_nn3==0)

```

```

{
  cluster_counter +=1; // Start a new cluster
  NodeL[i]=cluster_counter;
  NodeLP[cluster_counter]=cluster_counter;
} // end if (end case 4.2 (i))

// Case 4.2 (ii): There exists a labeled neighbour
else
{
  for (cn=0; cn<4; cn++) Num_cl[cn] = 0;
  cn = 0;
  //if the neighbour is already labeled (so it points to some cluster)
  and if it has an unbroken link with current monomer
  if (L_nn1!=0 && link1!=1) Num_cl[++cn] = NodeLP[L_nn1];
  if (L_nn2!=0 && link2!=1) Num_cl[++cn] = NodeLP[L_nn2];
  if (L_nn3!=0 && link3!=1) Num_cl[++cn] = NodeLP[L_nn3];

  if (cn==0) {
    cluster_counter +=1; %% Start a new cluster
    NodeL[i]=cluster_counter;
    NodeLP[cluster_counter]=cluster_counter;
  }
  else { // Put in the minimum labeling
    if (cn==1) NodeLPmin = NodeLP[Num_cl[1]];
    if (cn==2) NodeLPmin = min2(NodeLP[Num_cl[1]], NodeLP[Num_cl[2]]);
    if (cn==3) NodeLPmin = min3(NodeLP[Num_cl[1]], NodeLP[Num_cl[2]],
      NodeLP[Num_cl[3]]);

    NodeL[i] = NodeLPmin;
    for (i_cn=1; i_cn<=cn; i_cn++) NodeLP[Num_cl[i_cn]] = NodeLPmin;
  }
} // end else (end case 4.2 (ii))
} // end else (end case 4.2)
} // end for i
// STEP 5: RENUMBER LABELS IN NodeLP TO RUN SEQUENTIALLY
max_cluster_number = 0;
for (i=1; i<=cluster_counter; i++) {
  if(NodeLP[i] > max_cluster_number) {
    max_cluster_number ++;
    NodeLP[i] = max_cluster_number;
  }
}

// STEP 6: APPLY THE CORRECT LABELS TO THE ARRAY NodeL
for (i=0; i<N; i++) {
  if (i!=0) NodeL[i] = NodeLP[NodeL[i]];
}

// RECORD NUMBER OF CLUSTERS - NumberOfClusters - total number of clusters in
that configuration
NumberOfClusters = max_cluster_number;

/***** Perform Cluster Statistics *****/
// cluster_size[i] - gives the number of monomers in cluster_number "i"
// NC[i] - gives the total number of clusters of size "i"

for (i = 0; i <= N; i++) {NC[i] = 0; cluster_size[i] = 0;}

```

```

for (i = 0; i < N; i++) {
    if (NodeL[i] != 0) {
        cluster_number = NodeL[i];
        cluster_size[cluster_number] += 1;
    }
}

for (i = 1; i <= NumberOfClusters; i++) {
    num_mono = cluster_size[i];
    NC[num_mono] += 1.0;
}

//create histogram NC = probability distribution of cluster sizes
for(i=1; i<=N; i++) NC[i] /= NumberOfClusters;

return ;
}
/***** Auxiliary functions *****/
long min2(long x1, long x2)
{ // This function returns the minimum of two integer numbers
  if(x1<=x2) return(x1);
  else return(x2);
}
long min3(long x1, long x2, long x3)
{ // This function returns the minimum of three integer numbers
  if(x1<=x2 && x1<=x3) return(x1);
  else if (x2<=x1 && x2<=x3) return(x2);
  else return(x3);
}

```